Rare Metal Materials and Engineering
Volume 46, Issue 5, May 2017
Online English edition of the Chinese language journal

Available online at www.sciencedirect.com
ScienceDirect

Cite this article as: Rare Metal Materials and Engineering, 2017, 46(5): 1169-1175.

ARTICLE

One-pot Synthesis of Nano-$NiFe_2O_4$ Pinning on the Surface of the Graphite Composite as Superior Anodes for Li-ion Batteries

Hou Xianhua[1,2], Tang Xiaoqin[1], Hu Shejun[1,2], Wang Xinyu[1], Gao Yumei[3], Liu Xiang[1,4]

[1] Laboratory of Quantum Engineering and Quantum Materials, South China Normal University, Guangzhou 510006, China; *[2] Engineering Research Center of Materials & Technology for Electrochemical Energy Storage (Ministry of Education), Guangzhou 510006, China*; *[3] University of Electronic Science and Technology, Zhongshan 528400, China*; *[4] Nanjing University of Technology, Nanjing 210009, China*

Abstract: Nickel ferrite and related materials have recently received considerable attention as potential anode in lithium-ion batteries for their high theoretical specific capacities. To overcome low intrinsic electronic conductivity and large volume expansion during the Li insertion/extraction process, in this work, nano-$NiFe_2O_4$ pinning on the surface of the graphite composite was prepared by a hydrothermal method. As the superior anode material, the as-obtained nano-$NiFe_2O_4$/graphite composite demonstrates high capacity and excellent cycle stability. An initial specific discharge capacity of approximate 1478 mAh g^{-1} and a reversible specific capacity of approximate 1109 mAh g^{-1} after 50 cycles at a current density of 100 mA g^{-1} are reached. When the charging current is increased to 1000 mA g^{-1}, it also delivers a charge capacity of 750 mAh g^{-1}. The excellent performances are attributed to the special structure of $NiFe_2O_4$ nanoparticles pinning on the surface of the graphite, especially the enhanced electronic conductivity and area specific capacitance during the cycling process.

Key words: lithium ion batteries; anode material; nickel ferrite; composite materials; nanoparticles pining

Lithium-ion batteries have been considered as the most promising power source for electric vehicles (EVs), hybrid electric vehicles (HEVs) and mobile electronic devices. Among different anode materials, graphite is the conventional anode material for commercial lithium-ion batteries owing its low price, high conductivity, and high reversibility[1-3]. However, commercial graphite has already reached its theoretical limit (372 mAh g^{-1}), which restricts its further application in high-power systems such as EVs and HEVs[4-6]. Therefore, much attention has been paid to explore excellent alternative anode materials with high capacity, excellent cycling stability and rate capability.

Recently, many transition-metal oxide nanostructures, including Fe_2O_3[7,8], Fe_3O_4[9-11] and NiO[12,13], especially spinel transition-metal oxides $ZnFe_2O_4$[14-17], $NiFe_2O_4$[18-20] and $NiCo_2O_4$[21] have been extensively investigated due to their higher theoretical reversible capacities (~1000 mAh g^{-1}). It is well known that nanostructured materials can provide short diffusion pathways for lithium-ions, resulting in high rate capabilities. Among these oxides, nanostructured $NiFe_2O_4$ has been studied as a potential alternative anode because of its high theoretical capacity, low cost and low environmental impact. However, the large volume changes of the nickel ferrite anode during the continuous charge/discharge processes would lead to a poor capacity retention[18]. Particularly, such nanoparticles are likely to aggregate into larger particles that are pulverized again after long cycles, ultimately leading to rapid capacity fading. On the other hand, nanoparticles provide a large surface area over which a thick SEI layer can be formed easily and continuously with each charge/discharge cycle, resulting in a fast decline of reversible capacity.

Currently, a variety of nanostructures have been exploited

Received date: May 25, 2016
Foundation item: National Nature Science Foundation of China (51201066, 51171065); Natural Science Foundation of Guangdong Province (S2012020010937); Science and Technology Project Foundation of Zhongshan City of Guangdong Province (20123A326)
Corresponding author: Tang Xiaoqin, Master, Senior Engineer, Laboratory of Quantum Engineering and Quantum Materials, School of Physics and Telecommunication Engineering, South China Normal University, Guangzhou 510006, P. R. China, Tel: 0086-20-39318011, E-mail: houxh5697@163.com

for the purpose of increasing the cycling stability of ferrite electrodes, such as nanofibers structures[22], metal oxide/carbon composites[23,24], mesoporous structures[25,26], and inactive/active composites[27,28]. Among them, the nano-structured material/graphite composites may not only provide outstanding electron-conducting and ion-pathways, but also alleviate the mechanical stresses induced by the severe volume expansion during the cycling process[27,29]. To the best of our knowledge, the influences of graphite modification on the characteristics of the $NiFe_2O_4$ have not been reported yet. In this study, we reported a one-pot facile method to synthesize nano-$NiFe_2O_4$/graphite composite with outstanding electrochemical performance. The experimental results show that the $NiFe_2O_4$ nanoparticles are uniformly coated on the surface of stable graphite, which exhibit outstanding reversible capacity and cycling performance.

1 Experiment

The nano-$NiFe_2O_4$ was synthesized by a one-pot hydrothermal method. In a typical process, 8.66 g $FeCl_3$ $6H_2O$, 3.81 g $NiCl_2$.$6H_2O$, 10 g NH_4Ac, and 5 g citric acid were dissolved in 150 mL ethylene glycol with stirring for 1 h rapidly. Subsequently, the obtained precursor solution was transferred into the autoclave and heated to 200 ℃ for 24 h to get the precipitate. Then the resulting power was calcinated in an alumina crucible under N_2 atmosphere at 600 ℃ for 10 h and the nano-$NiFe_2O_4$ was obtained (sample 1). If 0.44 g graphite was added into the previous precipitate, mixing uniformity and the mixture was calcinated at 600 ℃ for 10 h in N_2, the nano-$NiFe_2O_4$/graphite composite was synthesized (sample 2). For comparison, 0.44 g graphite and other reactants were together dissolved in 150 mL ethylene glycol with stirring for 1 h, and the resulting solution was transferred into the autoclave and heated to 200 ℃ for 24 h. Finally, the precipitate was calcinated at 600 ℃ for 10 h in N_2 and the nano-$NiFe_2O_4$/graphite composite was also fabricated (sample 3).

Samples were characterized by XRD (XRD, PANalytical X' Pert PRO, Cu Kα, λ=0.154 06 nm). The laser Raman spectroscopy was investigated by an inVia (RENISHAW) laser Raman microscope. Morphology of samples was recorded by scanning electron microscopy (SEM, ZEISS ULTRA 55) and transmission electron microscopy (TEM, JEM-2100HR).

The electrochemical measurements were performed using coin-type half-cells (CR2530) assembled in an Ar-filled glove box. The working electrodes were prepared by mixing a slurry containing 80 wt% active material, 10 wt% Super P, and 10 wt% polyvinylidene fluoride (PVDF) binder. The electrolyte was 1 mol/L $LiPF_6$ in ethylene carbonate (EC), diethyl carbonate (DEC) and ethylene methyl carbonate (EMC) (1:1:1 by volume, provided by Chei Industries Inc., South Korea). A celgard 2400 was used as the separator. The charge/discharge measurements were performed using a LAND Celltest 2001A system in the voltage range of 0.001~3.0 V (versus Li^+/Li). The cycle voltammetry (CV) testing was carried out using Solartron Analytical 1470E system in the same voltage range at a constant scanning rate of 0.02 mV/s. Electrochemical impedance spectroscopy (EIS) measurements were studied on an electrochemical workstation (CHI 660B) with amplitude of 5 mV in the frequency range of 1 MHz to 0.01 Hz.

2 Results and Discussion

2.1 Structure analysis

The crystallographic structure and composition of the samples are determined by XRD. All the reflection peaks in Fig.1a could be indexed as $NiFe_2O_4$ with spinel structure (JCPDS No. 044-1485) and display a good crystallinity. The intensity of the peak belonging to the graphite phases at approximately 26.5° is rather obvious both in sample 2 and sample 3[6]. The peaks at 2θ of 30.3°, 35.7°, 63.0° can be assigned to the diffraction planes of (220), (311), (440) for $NiFe_2O_4$, respectively. In addition, no peaks corresponding to NiO or Fe_2O_3 are observed, which suggests that the chemical reaction of impurity crystalline phase are minimized by the hydrothermal method. It can be seen that the peaks of XRD pattern of sample 2 shown in Fig.1a are the same as those of sample 3. However, it also can be seen that the peaks of all samples are narrower especially the reflection of (311) crystal surface by conducting the calcination under inert gas atmosphere at 600 ℃. The results indicate that the crystallinity of the

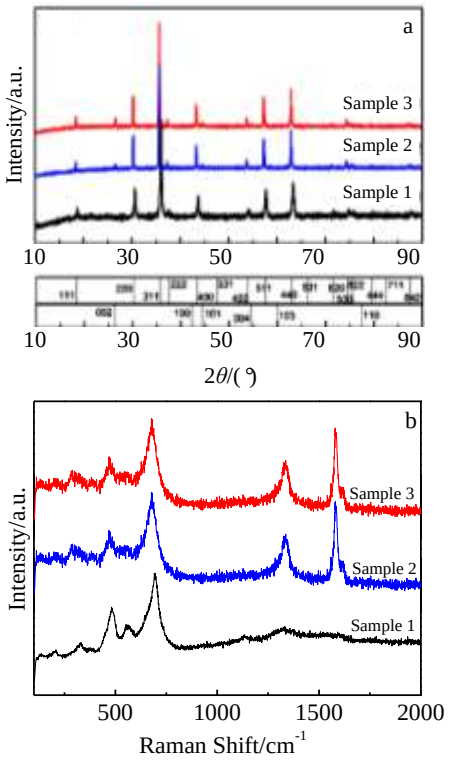

Fig.1 XRD patterns (a) and Raman spectra (b) of sample 1, sample 2 and sample 3

samples can be improved and the composition of samples is not changed seriously in the calcining process.

To further examine the effects of the graphite on the structure of nano-$NiFe_2O_4$, the Raman spectroscopy is presented in Fig. 1b. The peaks at 320, 480 and 700 cm^{-1} can be assigned to $NiFe_2O_4$ nanoparticles, while the other two distinguishable peaks at 1350 and 1600 cm^{-1} are assigned to graphite. It can be seen that sample 2 is also consistent with sample 3, which indicates that the presence of impurities can be negligible.

2.2 Morphology characterization

The SEM image in Fig. 2a shows the pure $NiFe_2O_4$ nanoparticles (sample 1). It is obvious that the $NiFe_2O_4$ nanoparticles are generally close to polyhedron structure with a high dispersion. It can also be seen that some of the larger nanoparticles have smaller nanoparticles growing on their surface. These small nanoparticles are interspersed between the larger ones indicating that the growth undergoes surface diffusion of nucleated crystals and coalescence of neighboring particles. Fig.2b shows morphology of nano-$NiFe_2O_4$/graphite composite (sample 2). For sample 2, graphite is added after hydrothermal reaction. It is clear that the $NiFe_2O_4$ nanoparticles are uniformly dispersed around the surface of stable graphite, but no pining occurs on it. However, the addition of graphite does not have obvious effects on the purity of $NiFe_2O_4$ nanoparticles (confirmed by XRD).

The morphology of as-obtained nano-$NiFe_2O_4$/graphite composite (sample 3) is shown in Fig. 2c. Because graphite is added before the hydrothermal reaction, $NiFe_2O_4$ nanoparticles are adhered firmly to the uneven surface of flake graphite, forming a thin layer, which is completely different from sample 2. The citric acid may serve as an adhesion agent between graphite and $NiFe_2O_4$. Giving an insight into Fig. 2c, sample 3 shows smaller particle size dispersion and larger surface area obviously than sample 2, which is not only be favorable for the Li^+ and electron transportation but also decreases the volume expansion during the charge/discharge process. So the special structure

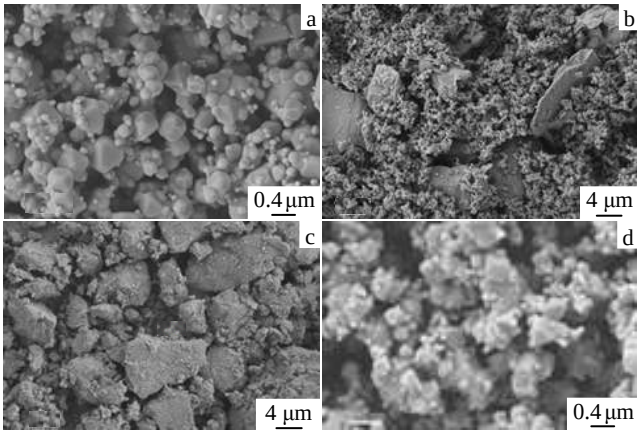

Fig. 2 SEM morphologies of sample 1 (a), sample 2 (b), and sample 3 (c, d)

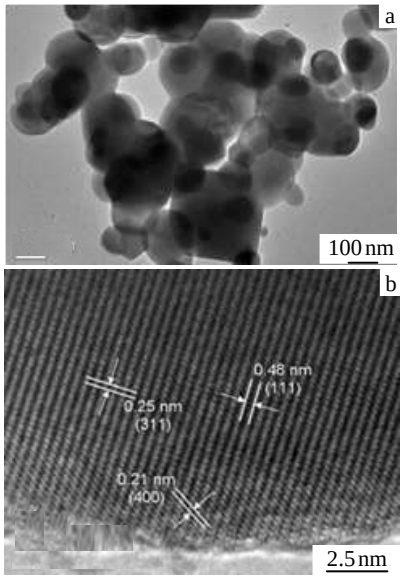

Fig. 3 TEM (a) and HRTEM (b) images of sample 3

of $NiFe_2O_4$ pinning on the surface of the graphite provides excellent electrical contact and constructs an expressway for ionic and electronic transport[23,29]. Moreover, the flake graphite also provides stable core for the pure $NiFe_2O_4$ nanoparticles to accommodate the mechanical strain induced by volume expansion during charge/discharge process.

Fig. 3a and 3b show the TEM image and HRTEM image of sample 3. It can be seen that the synthesized $NiFe_2O_4$ products are cubic nanoparticles with a size of about 300 nm. These $NiFe_2O_4$ nanoparticles are homogeneously pined on the surface of stable graphite in the nano-$NiFe_2O_4$/graphite composite. The clear lattice fringes with interplanar distances of 0.48, 0.25 nm and 0.21 nm are corresponded to the (111), (311) and (400) plan of $NiFe_2O_4$ cubic structure, respectively, implying the crystalline nature of $NiFe_2O_4$.

3 Electrochemical Properties

Fig. 4 shows the cycle voltammetry (CV) profiles of all samples in the voltage range of 0.01~3.0 V at a scan rate of 0.02 mV/s. In Fig.4a, the cathodic peaks below 0.2 V and the anodic peaks ranging from 0.15 to 0.45 V are associated with the intercalation/deintercalation of Li^+ with the graphite during the discharge/charge process[6]. Other peaks in Fig.4a are consistent with the traditional characteristics of $NiFe_2O_4$ CVs. In the first discharge cycle, two small peaks located at 0.7 V for sample 1 and 0.75 V for sample 2 can be ascribed to the formation of stable intermediate $Li_xNiFe_2O_4$ (Eq. 1). The following cathodic peaks associated with the reduction reaction of $NiFe_2O_4$ by Li are located at 0.5 V for sample 1 and sample 2 and 0.4 V for sample 3 (Eq. 2). According to Fig. 4a, it is obvious that the intermediate $Li_xNiFe_2O_4$ is not formed during the first discharge of sample 3 and the cathodic peak slightly shifts to 0.4 V. The positively shift should correspond to the

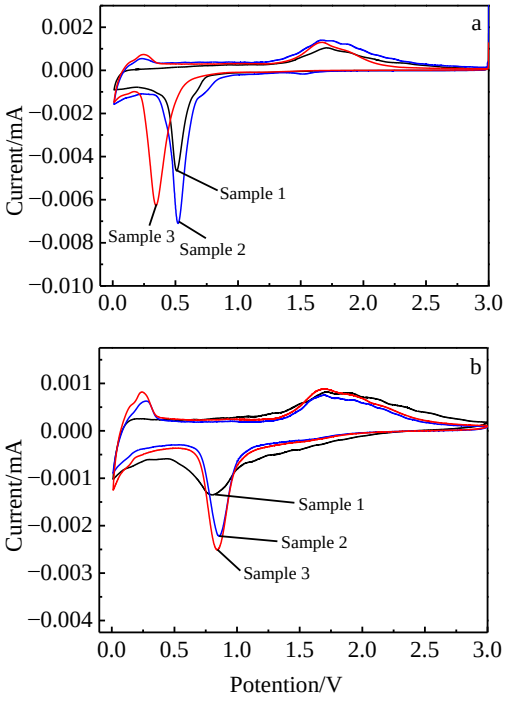

Fig.4 CV curves of sample 1, sample 2 and sample 3 at 1st cycle (a) and 10th cycle (b)

formation of intermediate $Li_xNiFe_2O_4$ and the polarization of the electrode materials. In order to investigate the further electrochemical reaction, the CV curves at the 10th cycle are shown in Fig.4b. It is clear that the redox peaks corresponding to the Ni/Ni^{2+} and Fe/Fe^{3+} redox couples are located at 0.75/1.75 V for sample 1 and 0.85/1.7 V for sample 2 and sample 3 (Eq.3). Remarkably, the area integrated within the CV curve of sample 3 is much larger than that of other samples, indicating that the nano-$NiFe_2O_4$/ graphite electrode (sample 3) has higher electrochemical reaction activity. It should be attributed to the special composite structure of graphite and polyhedral $NiFe_2O_4$.

$$NiFe_2O_4 + xLi^+ + xe^- \rightarrow Li_xNiFe_2O_4 \quad (1)$$

$$NiFe_2O_4 + 8Li^+ + 8e^- \rightarrow Ni + 2Fe + 4Li_2O \quad (2)$$

$$Ni + 2Fe + 4Li_2O \leftrightarrows NiO + Fe_2O_3 + 8Li^+ + 8e^- \quad (3)$$

The discharge/charge curves of the pure $NiFe_2O_4$ (sample 1) and $NiFe_2O_4$/graphite composites (sample 2 and sample 3) are shown in Fig.5 at a current density of 100 mA g^{-1}. The first discharge curves of the samples exhibit excellent initial discharge specific capacities of 1554 mAh g^{-1} (Fig.5a), 1417 mAh g^{-1} (Fig.5b) and 1478 mAh g^{-1} (Fig.5c), which are much larger than the theoretical value of $NiFe_2O_4$ (~1000 mAh g^{-1}). The extra reversible capacities can be attributed to the decomposition of organic electrolytes and the amorphization of the $NiFe_2O_4$ nanoparticles. Similar phenomena have been observed for other transition metal oxides[21,27]. The first discharge curve of sample 2 (Fig.5b) shows a smooth voltage decrease to 0.95 V firstly, and then a short plateau-like step at

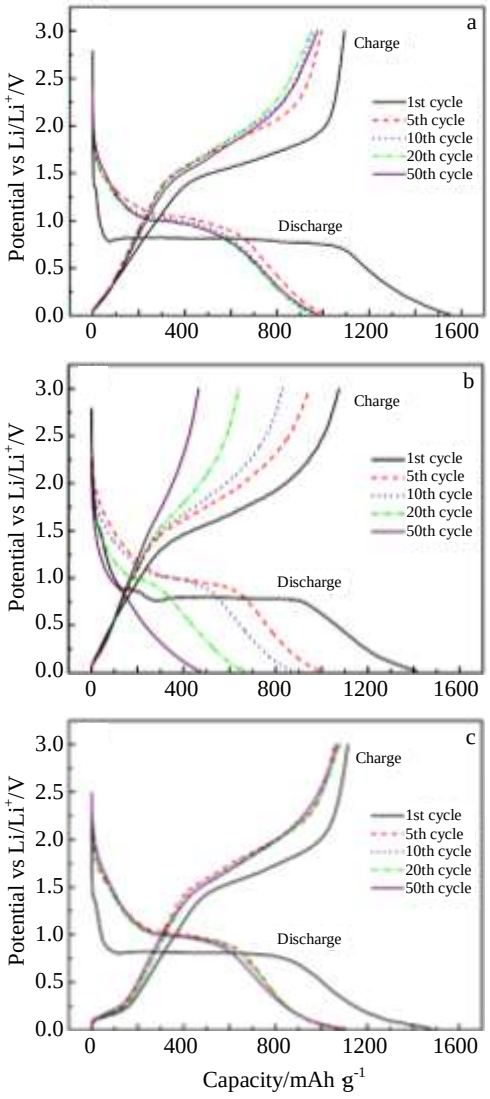

Fig.5 Charge/discharge curves of sample 1 (a), sample 2 (b) and sample 3 (c)

about 0.85 V, followed by a second drop ending at 0.8 V. According to the previous research, it can be attributed to reaction of $NiFe_2O_4 + xLi^+ + xe^- \rightarrow Li_xNiFe_2O_4$. Although the short plateau-like step of the first discharge curve of sample 1 is not obvious, it also performs a similar preceding intercalation process as sample 2 (Eq.1). Fig.5c shows the discharge and charge curves of sample 3. Compared with Fig. 5a and 5b, the voltage plateau at 0.8 V of sample 3 can be attributed to the reactions of $Ni^{2+} \rightarrow Ni$ and $Fe^{3+} \rightarrow Fe$. And the short plateau-like step is not observed during the first discharge process, which is consistent with the CV test.

The initial total capacities of samples are generally consistent with the additive contributions by mass fraction from $NiFe_2O_4$ and carbon matrix. The specific discharge and charge capacities of sample 2 in the initial cycle exhibit 1417 and 1075 mAh g^{-1}, respectively, making a coulombic efficiency

of 76%. For pure $NiFe_2O_4$, the first capacities are 1554 and 1092 mAh g^{-1}, respectively, making a lower coulombic efficiency of 70.3%. It is clear that the initial coulombic efficiency has been improved significantly with the addition of graphite. However, the charge capacities of sample 2 in the 5th, 10th, 20th and 50th cycles are 943, 830, 639 and 465 mAh g^{-1}, respectively, indicating that the discharge and charge capacities severely fade after the first cycle. As expected, the first coulombic efficiency of sample 3 is as high as 75.5% with the capacities of 1478 and 1116 mAh g^{-1}. In Fig.5a and 5c, it can also be seen that the reversible discharge capacities slightly increases from the 2nd cycle and reaches 981 mAh g^{-1} for the pure $NiFe_2O_4$ and 1109 mAh g^{-1} for the nano-$NiFe_2O_4$/graphite composite electrode after 50 cycles, which could be ascribed to the gradual activation of the graphite in the composite. Meanwhile, the decomposition of organic electrolytes and the amorphization of the $NiFe_2O_4$ nanoparticles after the charge/discharge process can also increase the capacities of nano-$NiFe_2O_4$/graphite composite. The results above demonstrate that the graphite could effectively improve the reversibility of the electrochemical reaction and initial coulombic efficiency, especially, mitigate the polarization of the electrode materials. Besides, the enhanced electrochemical performance of sample 3 can also be ascribed to the special structure of nano- $NiFe_2O_4$ pinning on the graphite, which not only decreases the volume expansion but also maintains the stable structure of the electrode during the cycling.

Fig. 6 illustrates the cycle performance of sample 1 and sample 3 at a current density of 100 mA g^{-1} for 50 cycles. It is obvious that the novel nano-$NiFe_2O_4$/graphite composite (sample 3) electrode is a compromise between the capacity and the cycle stability. Moreover, sample 3 exhibits much larger reversible capacity and better cyclability than sample 1 after 6th cycle. After 50 cycles, the capacity of sample 3 still keeps at 1109 mAh g^{-1}, which is 75% more than capacity of the first cycle. For comparison, the pure $NiFe_2O_4$ sample only keeps a capacity of 981 mAh g^{-1} after 50 cycles, about 63% capacity of the first cycle. This result indicates that the pining structures of $NiFe_2O_4$ nanoparticles and graphite significantly contribute to the cyclic stability. Remarkably, the cycling performance is largely enhanced in the nano-$NiFe_2O_4$/graphite composite electrode and is much better than that of other $NiFe_2O_4$-based nanostructures, such as SnO_2/ $NiFe_2O_4$ nanocomposites (710 mAh g^{-1} after 50 cycles)[18], $NiFe_2O_4$ nanoparticles (880 mAh g^{-1} after 30 cycles)[19], $NiFe_2O_4$-graphene nanocomposite (812 mAh g^{-1} after 50 cycles)[20] and $NiFe_2O_4$ nanofibers (900 mAh g^{-1} after 50 cycles)[22]. Thus, the unique $NiFe_2O_4$/graphite composite electrode exhibits good cycling stability with high specific capacitance.

The same result can also be seen from the rate capability of sample 1 and sample 3 (Fig.7). Sample 3 exhibits better rate capability between the two samples. When the charging current is increased from 50 to 1000 mA g^{-1}, it delivers charge

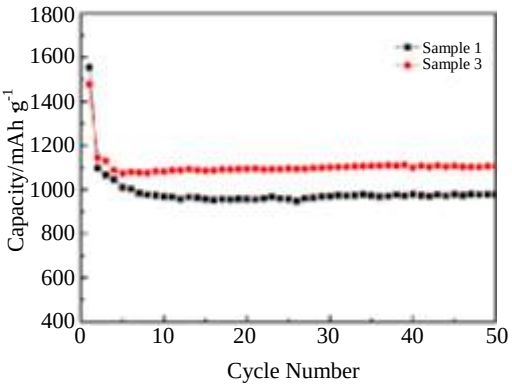

Fig.6 Cycle performance of sample 1 and sample 3

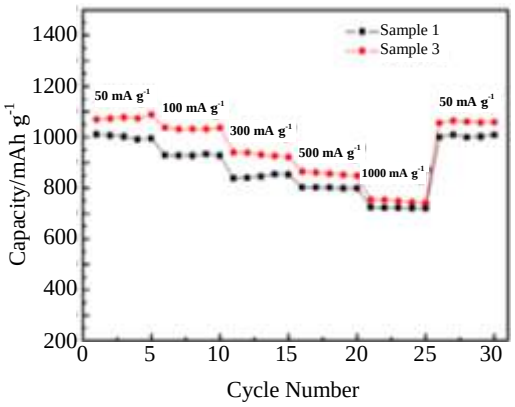

Fig.7 Rate capability of sample 1 and sample 3

capacities of 1080, 1030, 940, 860 and 750 mAh g^{-11}. However, when the current rises up to 1000 mA g^{-1}, the specific capacity of sample 1 is almost the same as that of sample 3 (730 mAh g^{-1}). Obviously, the rate capability improvement of sample 3 can be ascribed to that the graphite dramatically enhances the electronic conductivity of the $NiFe_2O_4$/graphite electrode and restrains the aggregation of nanoparticles.

To further study the influences of the graphite on the nano-$NiFe_2O_4$ electrode, EIS was conducted to indentify the relationship between the electrochemical performance and electrode kinetics. Fig.8 performs the Nyquist plots after the 2nd charge step. The impedance spectra of sample 1 and sample 3 are similar in the form with a semicircle at the high-to-medium frequency and a linear part at the lower frequency. In this case, the semicircle corresponds to the Faradic reactions and its diameter represents the interfacial charge-transfer impendence. Accordingly, the charge-transfer impendence of sample 3 is smaller than that of sample 1. In addition, the Warburg impedance in the low frequency refers to the electrolyte diffusion process. The slops of the straight line of two samples at the low frequency are almost the same, indicating that the two electrodes have the similar equal value of the electrolyte diffusion impedance. Apparently, the

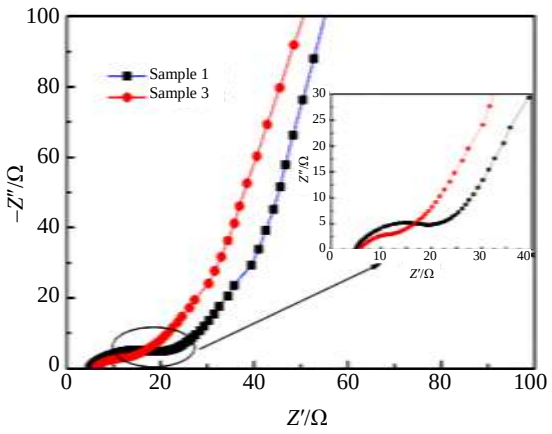

Fig.8 EIS plots of sample 1 and sample 3 (the inset shows the high frequency region)

excellent electrochemical performance of sample 3 is also attributed to the enhanced ion diffusion and low charge-transfer resistance.

The results all of above demonstrate that several factors are mainly responsible for the high specific capacitance and excellent cycling stability of the nano- $NiFe_2O_4$/graphite composite. Firstly, the well-distributed polyhedral $NiFe_2O_4$ nanoparticles enable easier electrolyte penetration into various regions of the material, increasing the utilization of the active materials and resulting in the good stability of electrode. Secondly, the graphite can increase the conductivity of electrode, ensure the fast charge- transportation and enhance the Li^+ diffusion rate during the discharge/charge process. Moreover, the graphite may also increase the surface area of nano-$NiFe_2O_4$/graphite composites, leading to a higher area specific capacitance. On the other hand, the graphite can also provide extra space for buffering the volume expansion, which would help to alleviate the structure damage and maintain the structural integrity of the electrode during the cycling process. Finally, the pinning structure between $NiFe_2O_4$ and graphite is beneficial for improving the initial efficiency and the cycling stability, suggesting the promising application of $NiFe_2O_4$/graphite composites in power LIBs.

4 Conclusions

1) The nano-$NiFe_2O_4$/graphite electrode synthesised by the one-pot hydrothermal method exhibits a high discharge capacity of 1478 mAh g^{-1} with superior cycling stability to the pure nano-$NiFe_2O_4$ electrode.

2) When the current density is increased from 50 to 1000 mA g^{-1}, the nano-$NiFe_2O_4$/graphite electrode delivers capacities of 1080 (50 mA g^{-1}), 1030 (100 mA g^{-1}), 940 (300 mA g^{-1}), 860 (500 mA g^{-1}) and 750 mAh g^{-1} (1000 mA g^{-1}).

3) The outstanding electrochemical performance of nano-$NiFe_2O_4$/graphite electrode is mainly attributed to the combination of polyhedral $NiFe_2O_4$ as well as graphite, which provides the increased electronic conductivity, faster ion transfer and better strain accommodation.

References

1 Ritchie A, Howard W. *Journal of Power Sources*[J], 2006, 162: 809
2 Si Q, Hanai K, Ichikawa T *et al*. *Journal of Power Sources*[J], 2010, 195: 1720
3 Ji L W, Lin Z, Alcoutlabia M *et al*. *Energy & Environmental Science*[J], 2011, 4: 2682
4 Yang J, Zhou X Y, Li J *et al*. *Materials Chemistry and Physics*[J], 2012, 135: 445
5 Nozaki H, Nagaoka K, Hoshi K *et al*. *Journal of Power Sources*[J], 2009, 194: 486
6 Li M, Hou X H, Sha Y J *et al*. *Journal of Power Sources*[J], 2014, 248: 721
7 Wang G, Liu T, Luo Y J *et al*. *Journal of Alloys and Compounds*[J], 2011, 509: L216
8 Du M, Xu C H, Sun J *et al*. *Journal of Materials Chemistry A*[J], 2013(1): 7154
9 Lee S H, Yu S H, Lee J E *et al*. *Nano Letters*[J], 2013, 13: 4249
10 He C N, Wu S, Zhao N Q *et al*. *ACS Nano*[J], 2013(7): 4459
11 Bayat M, Yang H, Ko F. *Polymer*[J], 2011, 52: 1645
12 Hwang S G, Kim G O, Yun S R *et al*. *Electrochimica Acta*[J], 2012, 78: 406
13 Jiang Y, Chen D D, Song J S *et al*. *Electrochimica Acta*[J], 2013, 91: 173
14 Deng Y F, Zhang Q M, Tang S D *et al*. *Chemical Communications*[J], 2011, 47: 6828
15 Song W T, Xie J, Liu S Y *et al*. *New Journal of Chemistry*[J], 2012, 36: 2236
16 Mueller F, Bresser D, Paillard E *et al*. *Journal of Power Sources*[J], 2013, 236: 87
17 Xing Z, Ju Z C, Yang J *et al*. *Nano Research*[J], 2012, 5: 477
18 Balaji S, Vasuki R, Mutharasu D. *Journal of Alloys and Compounds*[J], 2013, 554: 25
19 Kumar P R, Mitra S. *RSC Advances*[J], 2013(3): 25 058
20 Fu Y S, Wan Y H, Xia H *et al*. *Journal of Power Sources*[J], 2012, 213: 338
21 Liu X Y, Shi S J, Xiong Q Q *et al*. *ACS Applied Materials & Interfaces*[J], 2013, 5: 8790
22 Cherian C T, Sundaramurthy J, Reddy M V *et al*. *ACS Applied Materials & Interfaces*[J], 2013, 5: 9957
23 Wang Z, Zhang X, Li Y *et al*. *Journal of Materials Chemistry A*[J], 2013(1): 6393
24 Sui J H, Zhang C, Hong D *et al*. *Journal of Materials Chemistry*[J], 2012, 22: 13674
25 Gu X, Zhu W M, Jia C J *et al*. *Chemical Communications*[J], 2011, 47: 5337
26 Yao L M, Hou X H, Hu S J *et al*. *Journal of Solid State Electrochemistry*[J], 2013, 17: 2055
27 Liu S Y, Xie J, Zheng Y X *et al*. *Electrochimica Acta*[J], 2012, 66: 271

28 Xiao Y L, Zai J T, Tao L Q *et al*. *Physical Chemistry Chemical Physics*[J], 2013, 15: 3939

29 Yao L M, Hou X H, Hu S J *et al*. *Journal of Alloys and Compounds*[J], 2014, 585: 398

通过水热法合成的纳米铁酸镍/石墨复合阳极材料具有优异的电化学性能

侯贤华[1,2]，唐小琴[1]，胡社军[1,2]，王鑫瑜[1]，高玉梅[3]，刘　祥[1,4]

(1. 华南师范大学 广东省量子调控工程与材料重点实验室，广东 广州 510006)

(2. 教育部电化学储能材料与技术工程研究中心，广东 广州 510006)

(3. 电子科技大学，广州 中山 528400)

(4. 南京工业大学，江苏 南京 210009)

摘　要：作为锂离子电池阳极材料的铁酸镍及其相关材料，由于其具有较高的理论比容量，近来受到广泛关注。为了克服在充放电过程中的较低导电性与较大的体积膨胀等不良因素，通过水热法合成了纳米铁酸镍钉扎在石墨表面而形成的复合物。该纳米铁酸镍/石墨复合物表现出了较高的比容量以及优异的循环性能。其初始放电容量接近 1478 mAh g^{-1}，并且在 100 mA g^{-1} 的电流密度下循环 50 周之后，其可逆容量依然高达 1109 mAh g^{-1}。在 1000 mA g^{-1} 的充电电流情况下，该复合材料的充电容量也能保持 750 mA g^{-1}。这优异的电化学性能主要归功于纳米铁酸镍能够稳定的钉扎在石墨表面上，这种特殊的结构增强了材料的导电性同时也增大了材料的表面比容量。

关键词：锂离子电池；阳极材料；铁酸镍；复合材料；钉扎纳米颗粒

作者简介：侯贤华，男，1977 年生，博士，教授，华南师范大学物理与电信工程学院材料物理系，广东 广州 510006，电话：020-39318011，E-mail: houxh5697@163.com